Broadband circular polarization selector and converter based on multilayer metamaterials with stacked split-rings

Xiaojun Lin, Zhe Shen,* and Dingxin Huang
School of Electronic and Optical Engineering, Nanjing University of Science and Technology, Nanjing 210094, China

(Received 14 July 2023; accepted 15 December 2023; published 10 January 2024)

Metamaterial-based polarization devices are promising in imaging, sensing, and other applications. The balance between multifunction-achieved efficiency and their structural complexity has become an important issue to be discussed. In this paper, we proposed metamaterials with stacked gold split-rings as circular polarization selector and converter for broadband applications that operate in the near-infrared wavelength range. The circular polarization selector consists of six-layer stacked gold split-rings. It can transmit circularly polarized light with the same chirality as the structure and block the orthogonally polarized light. The circular polarization selector works with a bandwidth beyond 700 nm, and its figure of merit is over 11 000. Its operation band can be adjusted by changing the refractive index of the medium, and it has a wide-angle working capability. A circular polarization converter can be obtained by combining two circular polarization selectors with opposite chirality. It works in the range 1460–2100 nm, maintaining the polarization conversion ratio over 0.9 and the ellipticity angle above 20°. Furthermore, the corresponding physical mechanism was illustrated through the current analysis, and the reliability of the simulated results was verified by the theoretical calculation based on the transfer matrix method. The proposed metamaterial polarization devices can be used in optical communication, biomedicine, and other fields.

DOI: 10.1103/PhysRevMaterials.8.015203

I. INTRODUCTION

Circularly polarized light has unique features such as electromagnetic coupling, anisotropy, and circular dichroism ($CD = T_{RCP} - T_{LCP}$) [1–3]. It is widely used in quantum computation [4–6], optical communication [7], and liquid crystal display [8]. There are two traditional methods to generate circularly polarized light. One is combining a linear polarizer and a quarter-wave plate [9]. The other uses cholesteric liquid crystal films for Bragg reflection [10]. However, the conventional polarization elements are quite challenging to integrate into miniature photonic devices due to their large size, narrow bandwidth, and single function.

To date, the advances in metamaterials or metasurfaces have promoted the versatility and miniaturization of optical elements. They ensure high efficiency while widening the operation band, and have been used to realize circular polarizers [11–13] and asymmetric transmission devices [14–16]. Gansel *et al.* proposed helical nanostructure and achieved a broad bandwidth with CD up to 80%, opening an avenue for compact metamaterial circular polarizers [17]. Since then, double-helix, tapered-helix, and multihelix structures had been gradually proposed and verified to increase the extinction ratio ($ER = T_{RCP}/T_{LCP}$) and bandwidth [18–21]. The function of circular polarization conversion can also be realized by connecting two helical units with different orientations, with efficiency exceeding 75% [22]. To the best of our knowledge, helical structure has not been proven to achieve both polarization selection and conversion. These three-dimensional helical structures are prepared by laser direct writing or lithography technique, which are also challenging in production. Metamaterials with simplified helical structures were proposed to reduce fabrication complexity and retained relatively high performance [23–24]. Afterwards, multilayer metamaterials composed of nanofilms completely simplified the structure and greatly lowered fabrication difficulty, but inevitably led to a loss in efficiency [25–28]. Multilayer metamaterials have a relatively well-established mechanism. Both polarization selection and conversion can be obtained by rotating the upper layer of the structure [29] or combining two sets of rotating nanorods [30]. However, they still have much room for improvement in efficiency.

In this work, we proposed both a broadband circular polarization selector and a converter based on metamaterials. The metasurface selector is made of multilayer C-shaped split-ring resonators and retains the efficient performance of the helical structure. Split-ring was proposed by Sir Pendry *et al.* to realize a concept of negative-refractive-index metamaterial [31], which has been widely studied in recent decades [32–33]. Due to the chirality of the designed metamaterials, it is able to perform the function of polarization selection. By combining two circular polarization selectors with opposite chirality, a circular polarization convertor can be formed. For both selector and converter, we measured the functions of the designed metamaterials and evaluated their performance. Then we made current analysis and theoretical calculations by the transfer matrix method to clarify the physical mechanism. The proposed polarization devices may be very useful in optical communication and biomedical detection.

*Corresponding author: shenzhe@njust.edu.cn

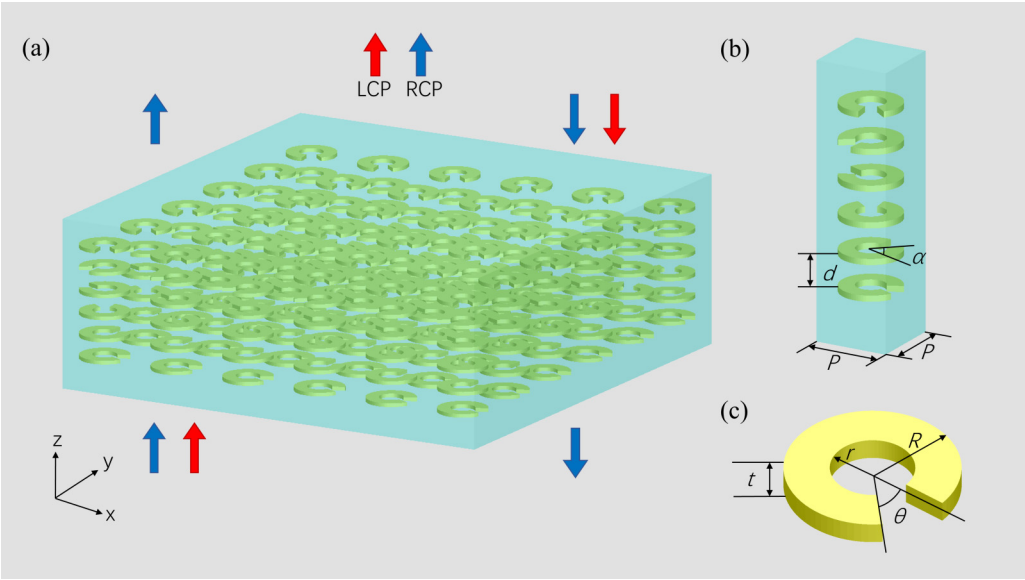

FIG. 1. (a) Schematic diagram of the proposed metamaterials for circular polarization selection. Red and blue arrows indicate the LCP and RCP light, respectively. (b) The diagram of the unit cell in the metamaterials. The distance between two adjacent split-rings $d = 130$ nm, and the relative rotation angle $\alpha = 60°$. The period of the unit cell $P = 300$ nm in both x and y directions. The refractive index of the medium $n = 1.2$. (c) The geometry of the single split-ring in the unit cell. The outer diameter $R = 125$ nm, the inner diameter $r = 60$ nm, the split angle $\theta = 45°$, and the thickness $t = 40$ nm.

II. CIRCULAR POLARIZATION SELECTOR

A. Metamaterial design

The diagram of our proposed metamaterials is presented in Fig. 1(a). For the forward propagation, the incident right-handed circularly polarized (RCP) light is transmitted with holding its original polarization state, but the left-handed circularly polarized (LCP) light is obstructed. The phenomena are the same for the backward incidence due to the symmetry of the structure along the light propagation direction. Therefore, the proposed metamaterials can be used for circular polarization selection. Figures 1(b) and 1(c) show the unit cell of the metamaterials and the single split-ring of the unit cell. The unit cell is composed of six-layer stacked gold split-rings with the same shape. Gold was chosen as the material because it does not have intrinsic solid losses in the near-infrared wavelength range and does not deteriorate with time [9]. The finite-difference time-domain (Lumerical, FDTD solutions) method was used to optimize parameters and make numerical calculations for simulating our metamaterials. Periodic boundary conditions were set along the x and y directions, and the perfectly matched layer (PML) condition was set along the z direction.

B. Function measurement

In order to measure the function of the designed metamaterials, the situation with the incidence of LCP and RCP light was simulated. The light was incident from the bottom of the metamaterials, and a monitor was placed at a certain distance above the structure to detect the transmitted light. As shown in Fig. 2(a), in the range 1500–2050 nm, the transmittance for RCP light is higher than 60% and up to 83.3%. On the contrary, the transmittance for LCP light in the range is

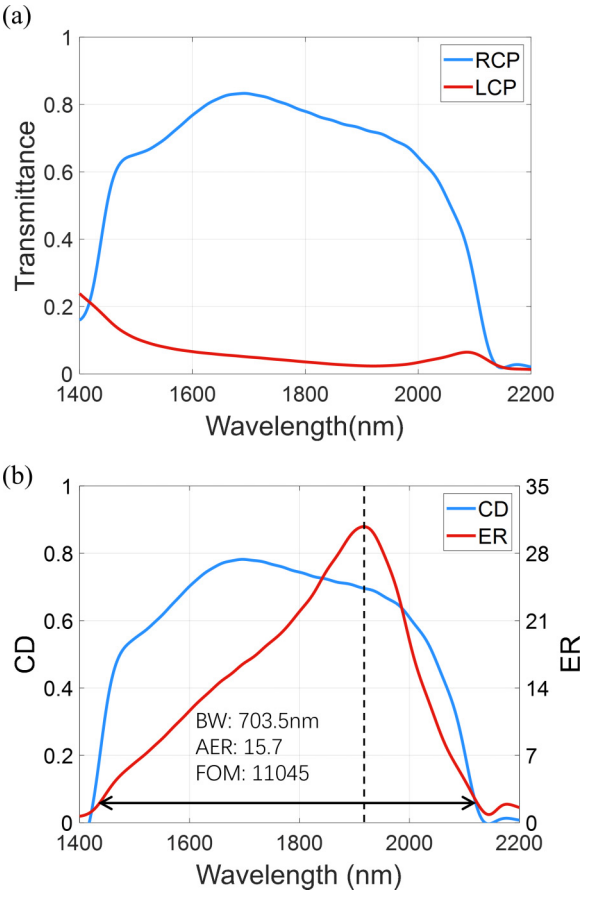

FIG. 2. (a) The transmittance curves of the proposed six-layer metamaterials. (b) The curves of CD and ER. The black dashed line corresponds to the wavelength of the maximum ER value, which is 1920 nm.

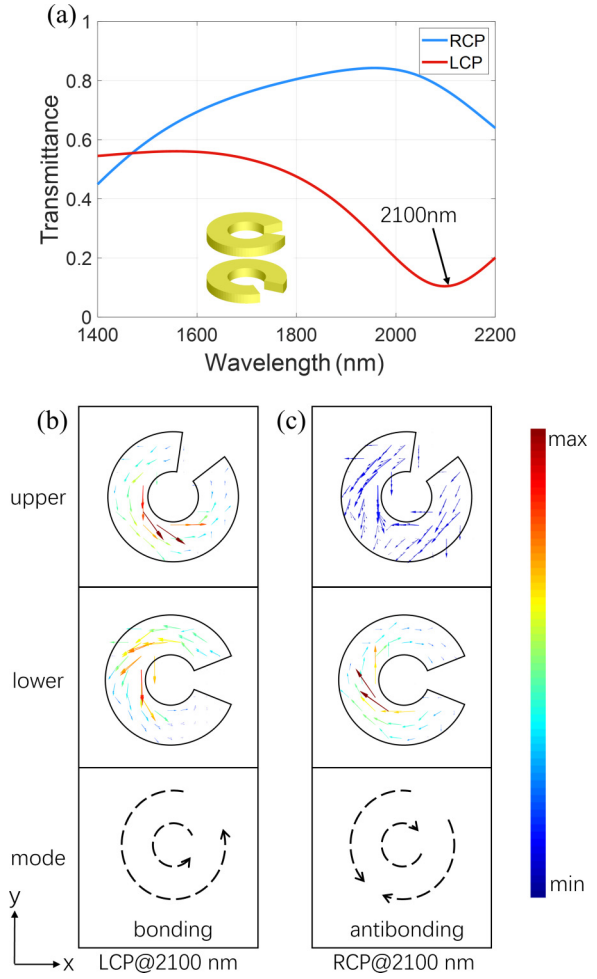

FIG. 3. (a) The transmittance curves of the bilayer split-rings. The current distributions and coupling modes of the bilayer split-rings at 2100 nm with (b) LCP and (c) RCP light incidence, respectively.

under 10%, which is much lower than that for RCP light. The huge difference in transmittance indicates that the majority of RCP light can be transmitted, while the LCP light is almost reflected. The CD and ER values were further calculated, as shown in Fig. 2(b). It can be seen that the CD is more than 50% in the range, and the ER reaches a maximum value of 31 at 1920 nm. Here, the figure of merit (FOM) is introduced to evaluate the performance of the proposed metamaterials. The operation bandwidth (BW) is defined as the wavelength range where the ER is larger than $\sqrt{2}$ [27], which is over 700 nm. Thus, the FOM is defined by the multiplication of the average ER (AER) and the operation bandwidth, which is more than 11 000. The high FOM indicates that the proposed metamaterials ensure a wide operation band as well as high distinction for the LCP and RCP light. Therefore, it can be used in optical communication to realize high-speed and low-noise multiplexing to improve the quality and capacity of information transmission.

C. Current analysis

To understand the potential physical mechanism of the proposed multilayer metamaterials, we started analysis from

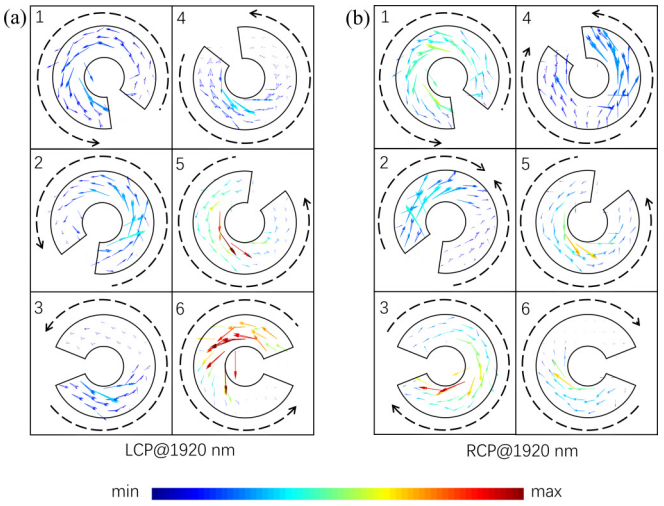

FIG. 4. The current distributions of the six-layer split-rings at 1920 nm with (a) LCP and (b) RCP light incidence, respectively.

the simplest bilayer case. Figure 3(a) plots the transmittance curves of the bilayer split-rings. It can be seen that the resonant dip at 2100 nm is excited by the incident LCP light. Then we analyzed the current distributions on the split-rings at this wavelength with different circularly polarized light incidence. Through Born-Kuhn modes in the hybridization model [14,34,35], the bilayer split-rings can be regarded as a coupled resonator system. Generally speaking, there are two basic modes in the hybridization model, i.e., the bonding mode comes from the symmetric alignment and the antibonding mode derives from the antisymmetric alignment. In Fig. 3(b), the current directions on the two split-rings are identical, indicating that the incident LCP light excites the lower energy level bonding mode, so that the majority of the LCP light is not absorbed but reflected. In Fig. 3(c), the induced currents with opposite directions occur in the overlapping part of the bilayer split-rings. It is because part of the incident RCP light is absorbed, leading to the excitation of antibonding mode. The bonding mode and the antibonding mode require different energies in the resonator system. Thus, the bilayer split-rings show a huge differential response for the two circularly polarized light and lead to a significant CD effect.

Based on the underlined mechanism in the bilayer case, we further analyzed the six-layer case. The split-rings are labeled from 1 to 6 in the order from the top to the bottom. Figures 4(a) and 4(b) show the current distributions on the split-rings for the LCP and RCP light incidence, respectively, at the wavelength of 1920 nm, where ER value is maximum. Obviously, the induced current appears on the bottom spilt-ring under the incidence of the LCP light, and transfers to the next upper layer by the magnetoelectric coupling between the split-rings. The current distributions on each adjacent bilayer split-rings can be regarded as the result of bonding mode individually, which is similar to the case in Fig. 3(b). Moreover, the current intensity on the split-rings tends to a weaker state, so that the incident LCP light is basically not transmitted. Under the incidence of the RCP light, the complex magnetoelectric coupling response appears on the split-rings. Similarly, the current distributions on each adjacent bilayer

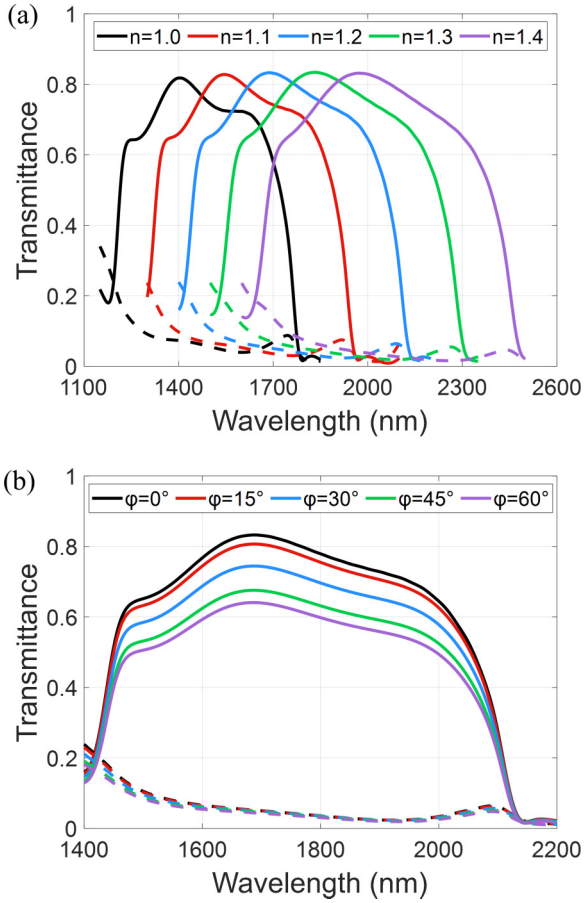

FIG. 5. The transmittance curves at different (a) refractive indices and (b) incidence angles. The solid and dashed lines indicate the transmittance for the incident RCP and LCP light, respectively.

split-rings can be regarded as the result of the antibonding mode individually, which is similar to the case in Fig. 3(c). The current analysis explains the coupling mechanism of the proposed metamaterials. Compared to the bilayer structure, the six-layer metamaterials exhibit a stronger CD response, and significantly widens the operation band.

D. Performance evaluation

In order to evaluate the performance of the proposed metamaterials, we explored the influence on the operation band at different medium refractive indices. As shown in Fig. 5(a), the transmittance curves were plotted with the medium refractive index varying 1–1.4. As the refractive index increases, the curve of the operation band shifts towards the long wavelength. The refractive index increases the optical path of light propagating in the medium, resulting in the resonance wavelength being redshifted. Meanwhile, the transmittance for the circularly polarized light decreases slightly, and the operation band expands from 600 to 800 nm. It is because the increase in the medium refractive index affects the charge density distributions on the metal surface, leading to a reduction of resonance intensity and an extension of the resonance band [36]. Therefore, it can be concluded that the operation band of the proposed metamaterials can be adjusted by changing

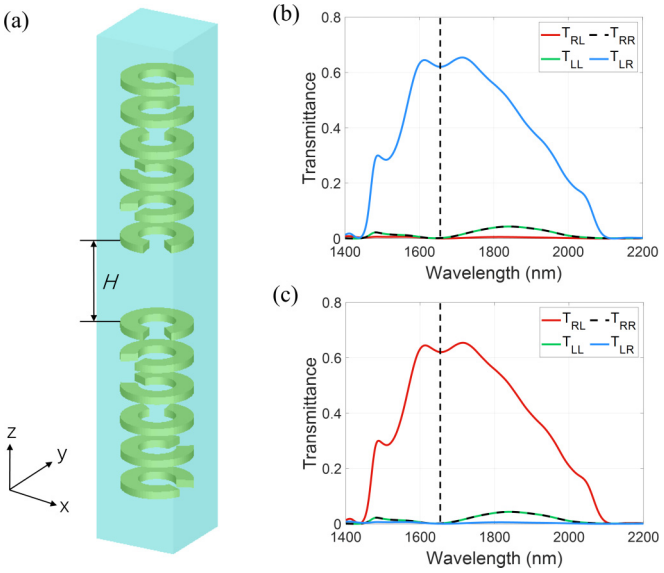

FIG. 6. (a) Schematic diagram of the unit cell in the proposed metamaterials for polarization conversion. The separation distance between two modules H= 450 nm. Other parameters are the same as in Fig. 1. Polarization transmission coefficients for (b) forward and (c) backward incidence. The subscripts "L" and "R" represent two orthogonal circular polarization states. $''T_{ij}''$ represents the conversion coefficient from circular polarization state $''j''$ to $''i.''$ The black dashed line corresponds to the wavelength with the highest polarization conversion ratio, which is 1640 nm.

the refractive index of the medium with high CD, which can be used in biomedicine to acquire information from multiple samples and provide convenience for the denoising process in information detection.

To verify the wide-angle working capability of the metamaterials, we further measured the transmission efficiency of the incident circularly polarized light at different incident angles. As shown in Fig. 5(b), the transmittance curves were plotted with the incident angle varying $0-60^{\circ}$ in steps of 15°. As the incident angle increases, the intensity of the incident light in the z direction reduces, and the transmittance for the incident light decreases accordingly, but still maintains high transmission performance. Moreover, the intrinsic chirality of the structure dominates here, so there is no need to consider the effect of extrinsic chirality. Therefore, the proposed metamaterials have a high tolerance for the incident angle, which can meet the need of a wide-angle working environment.

III. CIRCULAR POLARIZATION CONVERTER

A. Metamaterial design and function measurement

The concept of combining opposite chirality has been proposed to realize the electric and magnetic responses switching, handedness switching, and geometrical control of magnetic chirality [22,37–39]. In order to explore whether similar features exist in our metamaterials, we regarded the unit cell shown in Fig. 1(b) as a module, and its enantiomer with opposite chirality as the other module, then tried to combine them to form different metamaterials, as presented in Fig. 6(a). The bottom split-ring of the upper module and the top split-ring

of the lower module have the same spatial position in the x–y plane and are separated at a certain distance.

Since each module allows only one type of circularly polarized light to pass, it might be expected that both LCP and RCP light would be reflected. To verify this prediction, we simulated the transmission spectra in different incident directions. Figures 6(b) and 6(c) show the transmittance curves obtained by incident circularly polarized light along the $+z$ and $-z$ directions, respectively. It can be seen that the majority of the forward incident RCP light is converted to LCP light, and the incident LCP light is reflected. On the contrary, the backward incident LCP light is converted to RCP light, and the incident RCP light is almost obstructed. The backward incidence shows the opposite result because the upper and lower modules are mirror-symmetric. Surprisingly, no matter which direction the light comes from, there is always one type of circularly polarized light that can be transmitted. It is worth noting that the copolarization coefficients are close to 0 at the wavelength of 1640 nm, indicating that the copolarization transmission is very weak, and cross-polarization transmission is dominated at this wavelength. The high efficient polarization conversion can be used for information encoding and decoding to realize encrypted transmission.

Asymmetric transmission is an important characteristic in polarization conversion, which shows the difference in the coupling of metamaterials with different circularly polarized light in the transmission mode. It can be defined as the difference between the transmitted intensities for different propagation directions, which can be expressed as [40]

$$\Delta_{\mathrm{RCP}} = \left|T_{\mathrm{LR}}^{f}\right| - \left|T_{\mathrm{RL}}^{f}\right| = -\Delta_{\mathrm{LCP}}, \tag{1}$$

where the superscript f indicates forward incidence. Therefore, the asymmetric transmission coefficient of RCP and LCP light are calculated and presented in Fig. 7(a). The maximum asymmetric transmission parameter Δ_{RCP} is 0.65. In addition, Δ_{RCP} is above 0.4 in the range 1550–1900 nm. It can be inferred that the forward incident RCP light passes through the metamaterials and is converted, and the conversion of circularly polarized light in the backward incident direction is the opposite. The asymmetric transmission metamaterials provide a different way for the direction control of polarization transmission.

In order to further study the characteristic of the polarization converter, we calculated the polarization conversion ratio (PCR) according to the formula below:

$$\mathrm{PCR}_j = T_{ij}/(T_{ij} + T_{jj}), \tag{2}$$

where the subscripts i and j indicate RCP and LCP light, respectively, and the ellipticity angle χ of transmitted light is according to the following formula:

$$\chi = \frac{1}{2}\arcsin\left(\frac{2r}{1+r^2}\sin\Delta\varphi\right). \tag{3}$$

Here, r is the ratio of the amplitudes of the electric field intensity in the y and x directions. $\Delta\varphi$ is the phase difference between the electric field components in the y and x directions. According to Eqs. (2) and (3), PCR = 1 denotes complete polarization conversion, $\chi = 45^\circ$ or $\chi = -45^\circ$ denote that the light in transmitted fields are RCP or LCP light, respectively.

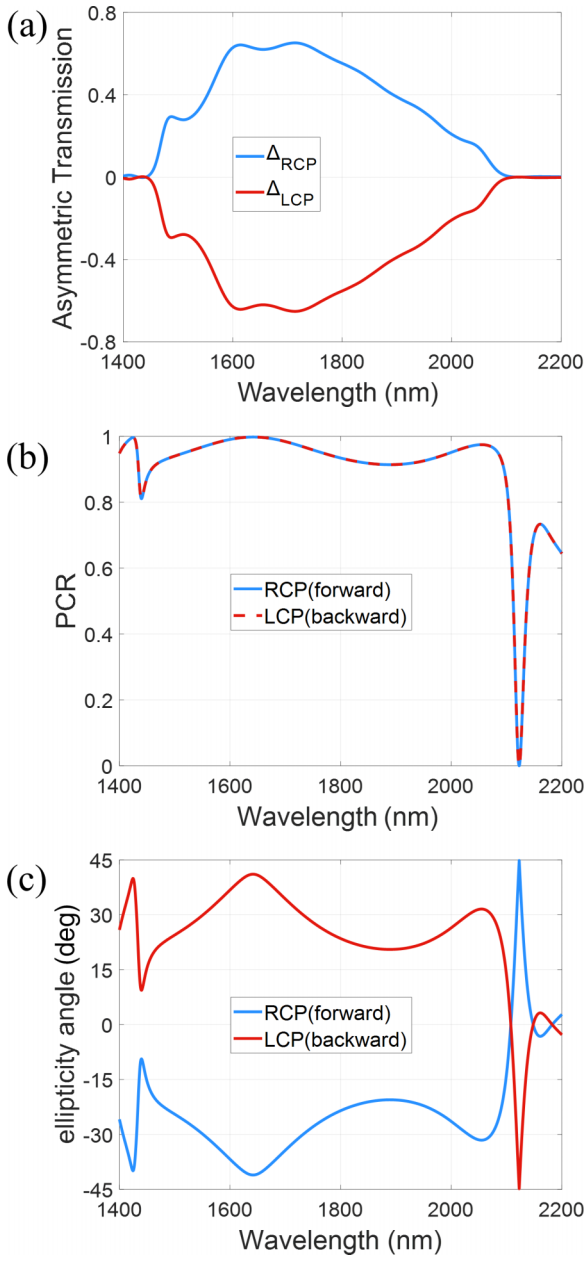

FIG. 7. Curves of (a) asymmetric transmission parameters, (b) PCR, and (c) ellipticity angle under forward incident RCP light and backward incident LCP light.

Figures 7(b) and 7(c) show the curves of the PCR and ellipticity angle, respectively. The PCR in the range 1460–2100 nm is higher than 0.9, and the absolute values of the ellipticity angle are above 20°, indicating that the conversion efficiency of the incident light is exceptionally high. Because of the weak copolarization for the incident light, the ellipticity angle cannot reach 45° ultimately. At 1640 nm, the PCR of both forward incident RCP light and backward incident LCP light is close to 1, and the ellipticity angle is 41°, indicating that the cross-polarization transmission is almost completed. The PCR is correlated with the conversion extent and the ellipticity angle is related to the polarization state of the transmitted light. The combination of high PCR and ellipticity angle

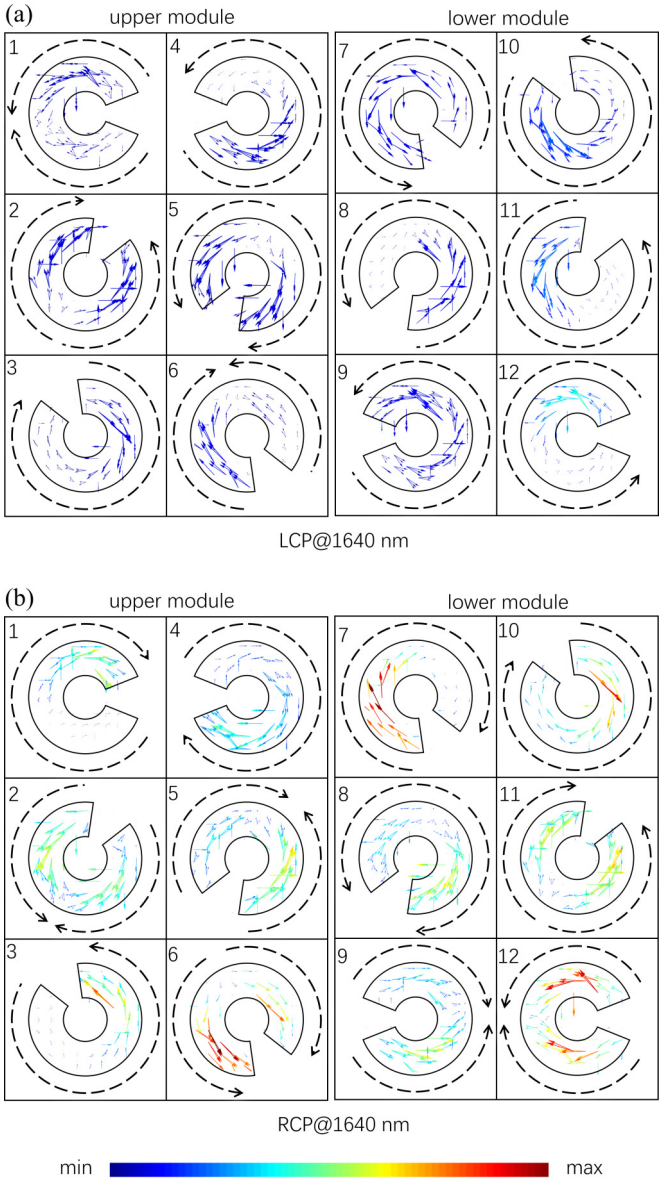

FIG. 8. The current distributions of the split-rings in the two modules at 1640 nm with (a) LCP and (b) RCP light incidence, respectively.

denotes that the proposed metamaterials can be used as a highly efficient photonics device.

B. Current analysis

Similarly, to further explore the potential physical mechanism of the metamaterial polarization converter, we analyzed the current distributions on the split-rings in the upper and lower modules. The split-rings are labeled from 1 to 12 in the order from the top to the bottom. Due to the symmetry of the structure, the situation of forward incidence was used as an example here. Figures 8(a) and 8(b) show the current distributions on the split-rings at 1640 nm, where the PCR is maximum, with the incident LCP and RCP light, respectively. Under the incidence of the LCP light, current with the same direction occurs on the all split-rings in the lower module. It is because the induced current generates on the bottom split-ring and then transfers to the upper layer with counterclockwise rotation. The phenomenon here is similar to that in Fig. 4(a). The difference is that the current distributions in the lower module are very weak, indicating that the incident LCP light is almost reflected. Under the incidence of the RCP light, a more complex magnetoelectric response occurs on the split-rings in the lower module, which is similar to the result in Fig. 4(b). Moreover, the strong induced currents appear on both the sixth and seventh split-rings, meaning that the incident RCP light flows between the two modules, and the polarization conversion is achieved after the interference of multiple transmission and reflection. However, due to the intrinsic ohmic loss of the multilayer gold split-rings, the final conversion efficiency is not very high. Combined with the results of current analysis, it reveals the potential mechanism of polarization conversion.

C. Theoretical calculations

The proposed multilayer metamaterials can be regarded as a Fabry-Perot-like cavity, so the total transmitted field results from the interference of multiple transmissions and reflections with the incident light. In order to verify the function of the proposed metamaterials, the transfer matrix method [41] was used to calculate the theoretical results of the multiple transmissions and reflections. First, we simulated and obtained the scattering parameters in the transmission and reflection matrices of each layer under forward and backward incidence. Then, we calculated 4×4 $\boldsymbol{M}_{\mathrm{ij}}$ matrices based on the obtained scattering parameters. $\boldsymbol{M}_{\mathrm{ij}}$ represents the transfer matrix of incident light from space j through the metamaterials to space i. The propagation through the homogeneous medium between layers is represented as the matrix $\boldsymbol{P}$:

$$P = \mathrm{diag}[\exp(ik_0nd), \exp(ik_0nd), \times \exp(-ik_0nd), \exp(-ik_0nd)], \quad (4)$$

where k_0 is the wave number in free space, n is the refractive index of the medium, and d is the distance between two adjacent layers. Therefore, for the proposed metamaterial circular polarization selector, the overall $\boldsymbol{M}$ matrix can be written as

$$\boldsymbol{M} = \boldsymbol{M}_{gf}\boldsymbol{P}\boldsymbol{M}_{fe}\boldsymbol{P}\boldsymbol{M}_{ed}\boldsymbol{P}\boldsymbol{M}_{dc}\boldsymbol{P}\boldsymbol{M}_{cb}\boldsymbol{P}\boldsymbol{M}_{ba}. \quad (5)$$

Finally, the four elements of the transmission matrix can be obtained from the $\boldsymbol{M}$ matrix. The method is also applied to the proposed metamaterial circular polarization converter.

Figures 9(b) and 9(c) show the theoretical calculation results of the proposed metamaterial selector and converter with dashed lines, respectively, which are basically consistent with the simulated results. Although the amplitudes of the theoretical and simulated results are slightly different, the curves largely overlap. The transfer matrix method does not consider the thickness of the metamaterials in the ideal condition. However, the excessive number of layers results in that the thickness cannot be ignored, thus small discrepancies occur in the theoretical results, but it is still acceptable. The basic coincidence of theoretical and simulated results further verifies the reliability of our work.

Before making a conclusion, we elucidate the similarities and differences among our work and others [34,42–45] that used layered split-ring resonators in terms of structural design,

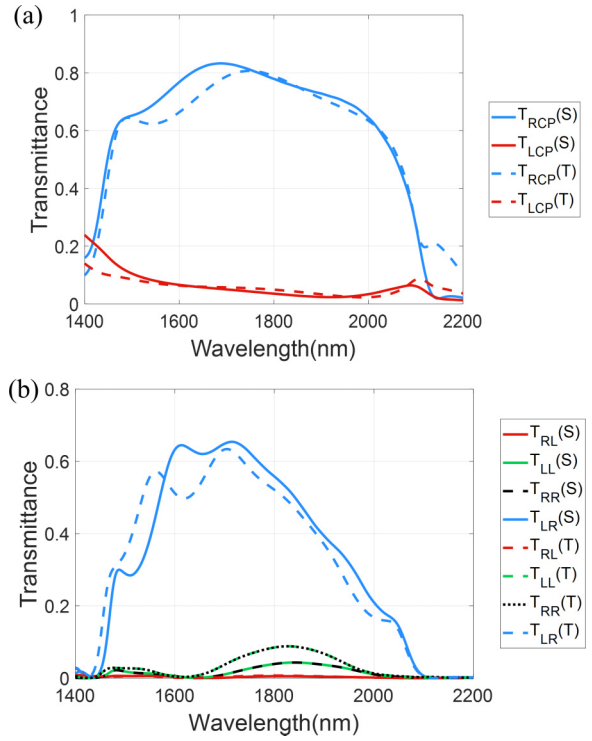

FIG. 9. Simulated (marked with *S*) and theoretical (mark with *T*) transmittance curves of the proposed metamaterial (a) polarization selector and (b) polarization converter.

mechanisms, and optical properties, as shown in Table I. It can be seen that split-ring resonators have been used to design various systems to realize different optical properties, which have been explained by a few main mechanisms including current analysis and electric and magnetic coupling. Our work introduces the optical properties of circular polarization selection and conversion containing the mechanisms of current analysis and chirality, which are different from previous ones.

IV. CONCLUSION

In conclusion, we proposed metamaterials with stacked gold split-rings as broadband circular polarization selector and converter. The operation bandwidth of the circular polarization selector is over 700 nm, with the the FOM over 11 000. The selector can be used for sensing and wide-angle operation. The circular polarization converter has efficient asymmetric transmission in the range 1550–1900 nm, with a high PCR and ellipticity angle. The current analysis confirms the corresponding physical mechanism of the metamaterial polarization selector and converter. Furthermore, the results of the theoretical calculation verified the reliability of the simulated results. In short, the broadband circular polarization selector and converter proposed in this work have great potential in integrated photonic devices, optical sensors, and so on.

ACKNOWLEDGMENTS

This work was supported by National Natural Science Foundation of China (Grants No. 62275122 and No. 61805119); Natural Science Foundation of Jiangsu Province (Grants No. BK20180468 and No. BK20180469); Fundamental Research Funds for the Central Universities (Grant No. 30919011275).

TABLE I. The comparison of our proposed metamaterials and other layered split-ring resonators.

References	Structural design	Mechanisms	Optical properties
[34]	double-layered U-shaped resonators	current analysis, electric and magnetic interactions	amplitude modulation
[42]	double-layered U-shaped resonators	current analysis, electric and magnetic dipoles coupling	negative refractive index
[43]	double-layered four U-shaped resonators	electric and magnetic coupling	polarization rotation
[44]	double-layered four U-shaped resonators	current analysis, electric and magnetic coupling	negative refractive index, circular dichroism, polarization rotation
[45]	double-layered U-shaped resonators	current analysis, magnetic resonance	polarization rotation
Our work	6-layered C-shaped resonators, 12-layered C-shaped resonators	current analysis, chirality	circular polarization selection and conversion

[1] M. Decker, M. W. Klein, M. Wegener, and S. Linden, Circular dichroism of planar chiral magnetic metamaterials, Opt. Lett. **32**, 856 (2007).

[2] D. H. Kwon, P. L. Werner, and D. H. Werner, Optical planar chiral metamaterial designs for strong circular dichroism and polarization rotation, Opt. Express **16**, 11802 (2008).

[3] A. B. Khanikaev, N. Arju, Z. Fan, D. Purtseladze, F. Lu, J. Lee, P. Sarriugarte, M. Schnell, R. Hillenbrand, M. A. Belkin, and G. Shvets, Experimental demonstration of the microscopic origin

of circular dichroism in two-dimensional metamaterials, Nat. Commun. **7**, 12045 (2016).

[4] J. F. Sherson, H. Krauter, R. K. Olsson, B. Julsgaard, K. Hammerer, I. Cirac, and E. S. Polzik, Quantum teleportation between light and matter, Nature (London) **443**, 557 (2006).

[5] C. Wagenknecht, C. M. Li, A. Reingruber, X. H. Bao, A. Goebel, Y. A. Chen, Q. A. Zhang, K. Chen, and J. W. Pan, Experimental demonstration of a heralded entanglement source, Nat. Photonics **4**, 549 (2010).

[6] E. Togan, Y. Chu, A. S. Trifonov, L. Jiang, J. Maze, L. Childress, M. V. G. Dutt, A. S. Sorensen, P. R. Hemmer, A. S. Zibrov, and M. D. Lukin, Quantum entanglement between an optical photon and a solid-state spin qubit, Nature (London) **466**, 730 (2010).

[7] R. Farshchi, M. Ramsteiner, J. Herfort, A. Tahraoui, and H. T. Grahn, Optical communication of spin information between light emitting diodes, Appl. Phys. Lett. **98**, 162508 (2011).

[8] M. Xu, F. Xu, and D.-K. Yang, Effects of cell structure on the reflection of cholesteric liquid crystal displays, J. Appl. Phys. **83**, 1938 (1998).

[9] Y. H. Huang, Y. Zhou, and S. T. Wu, Broadband circular polarizer using stacked chiral polymer films, Opt. Express **15**, 6414 (2007).

[10] Z. Z. Zhuang, Y. J. Kim, and J. S. Patel, Behavior of the cholesteric liquid-crystal Fabry-Perot cavity in the Bragg reflection band, Phys. Rev. Lett. **84**, 1168 (2000).

[11] J. H. Shi, Q. C. Shi, Y. X. Li, G. Y. Nie, C. Y. Guan, and T. J. Cui, Dual-polarity metamaterial circular polarizer based on giant extrinsic chirality, Sci. Rep. **5**, 16666 (2015).

[12] Z. C. Li, W. W. Liu, H. Cheng, S. Q. Chen, and J. G. Tian, Spin-selective transmission and devisable chirality in two-layer metasurfaces, Sci. Rep. **7**, 8204 (2017).

[13] S. Y. Yang, Z. Liu, S. Hu, A. Z. Jin, H. F. Yang, S. Zhang, J. J. Li, and C. Z. Gu, Spin-selective transmission in chiral folded metasurfaces, Nano Lett. **19**, 3432 (2019).

[14] Y. H. Cui, L. Kang, S. F. Lan, S. Rodrigues, and W. S. Cai, Giant Chiral Optical Response from a Twisted-Arc Metamaterial, Nano Lett. **14**, 1021 (2014).

[15] T. J. Guo and C. Argyropoulos, Broadband polarizers based on graphene metasurfaces, Opt. Lett. **41**, 5592 (2016).

[16] Y. Ren, C. Jiang, and B. Tang, Asymmetric transmission in bilayer chiral metasurfaces for both linearly and circularly polarized waves, J. Opt. Soc. Am. B **37**, 3379 (2020).

[17] J. K. Gansel, M. Thiel, M. S. Rill, M. Decker, K. Bade, V. Saile, G. von Freymann, S. Linden, and M. Wegener, Gold helix photonic metamaterial as broadband circular polarizer, Science **325**, 1513 (2009).

[18] Z. Y. Yang, M. Zhao, P. X. Lu, and Y. F. Lu, Ultrabroadband optical circular polarizers consisting of double-helical nanowire structures, Opt. Lett. **35**, 2588 (2010).

[19] S. X. Li, Z. Y. Yang, J. Wang, and M. Zhao, Broadband terahertz circular polarizers with single- and double-helical array metamaterials, J. Opt. Soc. Am. A **28**, 19 (2011).

[20] J. K. Gansel, M. Latzel, A. Frolich, J. Kaschke, M. Thiel, and M. Wegener, Tapered gold-helix metamaterials as improved circular polarizers, Appl. Phys. Lett. **100**, 101109 (2012).

[21] S. Behera and J. Joseph, N-single-helix photonic-metamaterial based broadband optical range circular polarizer by induced phase lags between helices, Appl. Opt. **54**, 1212 (2015).

[22] J. Kaschke, L. Blume, L. Wu, M. Thiel, K. Bade, Z. Y. Yang, and M. Wegener, A helical metamaterial for broadband circular polarization conversion, Adv. Opt. Mater. **3**, 1411 (2015).

[23] R. N. Ji, S. W. Wang, X. X. Liu, X. S. Chen, and W. Lu, Broadband circular polarizers constructed using helix-like chiral metamaterials, Nanoscale **8**, 14725 (2016).

[24] J. P. Hu, X. N. Zhao, R. B. Li, A. J. Zhu, L. H. Chen, Y. Lin, B. Cao, X. J. Zhu, and C. H. Wang, Broadband circularly polarizing dichroism with high efficient plasmonic helical surface, Opt. Express **24**, 11023 (2016).

[25] Y. Zhao, M. A. Belkin, and A. Alu, Twisted optical metamaterials for planarized ultrathin broadband circular polarizers, Nat. Commun. **3**, 870 (2012).

[26] X. W. Yan, M. D. Zhang, K. L. Ren, J. H. Liu, W. W. Zhang, and J. Dong, Tunable broadband circular polarizer based on ultrahigh-order surface plasmonic resonance, Appl. Opt. **58**, 2854 (2019).

[27] M. D. Zhang, Q. N. Lu, J. Xu, and B. Z. Ge, Broadband circular polarizer based on twisted plasmonic nano-disks, Appl. Opt. **58**, 4846 (2019).

[28] C. Pfeiffer, C. Zhang, V. Ray, L. J. Guo, and A. Grbic, High performance bianisotropic metasurfaces: Asymmetric transmission of light, Phys. Rev. Lett. **113**, 023902 (2014).

[29] Y. Y. Kang, D. F. Tang, and J. F. Dong, Conversion of near-infrared polarization characteristics by rotation of the upper layer in a three-layer structure, J. Opt. **20**, 095101 (2018).

[30] S. E. Mun, J. Hong, J. G. Yun, and B. Lee, Broadband circular polarizer for randomly polarized light in few-layer metasurface, Sci. Rep. **9**, 2543 (2019).

[31] J. B. Pendry, A. J. Holden, D. J. Robbins, and W. J. Stewart, Magnetism from conductors and enhanced nonlinear phenomena, IEEE Trans. Microwave Theory Tech. **47**, 2075 (1999).

[32] N. Liu, S. Kaiser, and H. Giessen, Magnetoinductive and electroinductive coupling in plasmonic metamaterial molecules, Adv. Mater. **20**, 4521 (2008).

[33] Z. Wei, Y. Zhao, Y. Zhang, W. Cai, Y. Fan, Z. Wang, and X. Cheng, High-efficiency modulation of broadband polarization conversion with a reconfigurable chiral metasurface, Nano. Adv. **4**, 4344 (2022).

[34] N. Liu, H. Liu, S. Zhu, and H. Giessen, Stereometamaterials, Nat. Photonics **3**, 157 (2009).

[35] X. Yin, M. Schäferling, B. Metzger, and H. Giessen, Interpreting chiral nanophotonic spectra: The plasmonic Born–Kuhn model, Nano Lett. **13**, 6238 (2013).

[36] G. Mie, Beiträge zur Optik trüber Medien, speziell kolloidaler Metallösungen, Ann. Phys. **330**, 377 (1908).

[37] X. Xiong, W. H. Sun, Y. J. Bao, R. W. Peng, M. Wang, C. Sun, X. Lu, J. Shao, Z. F. Li, and N. B. Ming, Switching the electric and magnetic responses in a metamaterial, Phys. Rev. B **80**, 201105 (2009).

[38] S. Zhang, J. Zhou, Y. S. Park, J. Rho, R. Singh, S. Nam, A. K. Azad, H. T. Chen, X. Yin, A. J. Taylor, and X. Zhang, Photoinduced handedness switching in terahertz chiral metamolecules, Nat, Commun. **3**, 942 (2012).

[39] D. Sanz Hernandez, A. Hierro Rodriguez, C. Donnelly, J. Pablo Navarro, A. Sorrentino, E. Pereiro, C. Magen, S. McVitie, J. M. de Teresa, S. Ferrer, P. Fischer, and A. Fernandez Pacheco, Artificial double-helix for geometrical control of magnetic chirality, ACS Nano. **14**, 8084 (2020).

[40] C. Menzel, C. Rockstuhl, and F. Lederer, Advanced Jones calculus for the classification of periodic metamaterials, Phys. Rev. A **82**, 053811 (2010).

[41] Z. Shen and Q. He, Mutual circular polarization conversions in asymmetric transmission and reflection modes by three-layer metasurface with gold split-rings, Opt. Express **29**, 34850 (2021).

[42] X. Xiong, W. H. Sun, Y. J. Bao, M. Wang, R. W. Peng, C. Sun, X. Lu, J. Shao, Z. F. Li, and N. B. Ming, Construction of a chiral metamaterial with a U-shaped resonator assembly, Phys. Rev. B **81**, 075119 (2010).

[43] A. Andryieuski, C. Menzel, C. Rockstuhl, R. Malureanu, F. Lederer, and A. Lavrinenko, Homogenization of resonant chiral metamaterials, Phys. Rev. B **82**, 235107 (2010).

[44] Z. Li, R. Zhao, T. Koschny, M. Kafesaki, K. B. Alici, E. Colak, H. Caglayan, E. Ozbay, and C. M. Soukoulis, Chiral metamaterials with negative refractive index based on four "U" split ring resonators, Appl. Phys. Lett. **97**, 081901 (2010).

[45] X. Liu, Y. Xu, Z. Zhu, S. Yu, C. Guan, and J. Shi, Manipulating wave polarization by twisted plasmonic metamaterials, Opt. Mater. Express **4**, 1003 (2014).